The Modeling and Numerical Solution of Branch Retinal Artery Occlusion

Fatahillah, A.*[1,2], Widodo, B.[1], and Roslan, R.[3]

[1]*Department of Mathematics, Sepuluh Nopember Institute of Technology, Surabaya, Indonesia*
[2]*Department of Mathematics Education, University of Jember, Jember, Indonesia*
[3]*Department of Mathematics and Statistics, Faculty of Applied Sciences and Technology,
Universiti Tun Hussein Onn Malaysia, Pagoh Campus, 84600 Muar, Johor, Malaysia*

E-mail: fatahillah767@gmail.com
*Corresponding author

Abstract

The diameter of an artery can narrow due to blood clots or accumulations of cholesterol obstructing blood flow in one or more retinal arteries, leading to the occurrence of Retinal Artery Occlusion (RAO) and painless vision loss. This study introduces a mathematical model to analyze blood flow in Branch Retinal Artery Occlusion (BRAO). Built using the Finite Volume Method (FVM), the model included variability in its geometric (thickness and length of constriction) and three-dimensional topological structures. The model was developed using the QUICK method and simulated to determine the effect of stenosis and initial flow velocity on the emergence of eye stroke with the aid of MATLAB. This simulation documented the magnitude of velocity and pressure for various forms of stenosis to analyze the causes of eye stroke. Computational Fluid Dynamics was employed to simulate turbulent flow in BRAO using ANSYS FLUENT. The results show that 90% thickness clot in a branch of the retinal artery can be extremely dangerous because the flow rate and pressure exceed normal limits. With the increased severity of stenosis, the pressure and wall shear stress at the stenosis region also increase, eventually and the high-speed flow rate formed at the stenosed region begins to dominate the flow. The conclusion of present study is relevant to the investigation of disease arteries and has contributed to a more fine-cut understanding of the impact of BRAO on eye stroke.

Keywords: modelling; finite volume method; branch retinal artery occlusion.

1   Introduction

The Joint National Committee for the Prevention, Detection, Evaluation, and Treatment of High Blood Pressure (JNC VI) [5] and the World Health Organization and the International Society of Hypertension (WHO-ISH) [22] have acknowledged that a person with a systolic pressure of 130 to 139 mm Hg and a diastolic pressure of 85 to 89 mm Hg is identified to have a normal high blood pressure. High blood pressure can damage the arteries that carry blood to the eyes. When blood clots or accumulations of cholesterol obstruct blood flow in one or more retinal arteries, Retinal Artery Occlusion (RAO) will emerge. Although rare, RAO can cause painless vision loss [18, 27]. Similar to common stroke that affects our brain, this incident is indicated by the block of blood flow in the eyes. Apart from the brain, strokes can also occur in the eyes due to blockage of blood vessels in the retina, resulting in an abrupt decline in visual acuity and even permanent blindness. One of the causes of this disease is clots in the blood vessels of the eye's retina. Eye strokes can be caused by blood clots in the retina. Apart from that, this blockage can also occur when plaque blocks the retinal blood vessels. Blockage may occur in the main artery or its branches. The geometry of stenosis affects blood flow in the arteries, depending on the shape, length, and height of the stenosis.

Therefore, mathematical studies on such situations are important to investigate [1]. Retinal ischemia can occur either temporarily or permanently due to branch retinal artery occlusion (BRAO) or central retinal artery occlusion (CRAO) [13] refer to Figures 1 and 2. BRAO is a common ocular vascular occlusion disorder [16]. Diseases associated with arterial stenosis play an essential role in hemodynamics because they disrupt flow patterns, which cause variations in wall pressure and wall shear stress in the arteries [4]. The diagnosis of BRAO is based on various clinical findings. First, there is a history of a sudden decrease in eye vision. Another finding is concerned with initial ophthalmic evaluation, which is associated with acute retinal ischemia in the distribution of the occluded retinal artery branches. Finally, based on an invasive diagnostic procedure in this study, there is no clear circulation in the involved retinal artery branch, except in eyes with transient BRAO [13, 12].

Figure 1: Color fundus of the right eye with supero-temporal branch retinal artery occlusion [12, 14].

Many studies have focused on retinal artery stenosis. Lauda et al. [16] conclude that acute brain infarction occurred in 23% of 213 BRAO patients. This finding has further substantiated that vision loss is the only symptom identified in 90% of these patients. Another study conducted by Lavallee et al. [17] underscores that ischemia is a causative factor in 93.3% of Transient Ischemic Attack (TIA) patients who experience monocular vision loss. In addition, Pinna [23] reports that

approximately 60% of the patients with simultaneous BRAO and Central Retinal Vein Occlusion (CRVO) are at risk of vascular complications. Notwithstanding, these studies have yet to detect the simultaneous effects of the degree of constriction and the initial velocity of the flow on the fluid flow pattern. The present study aims to address this gaping void.
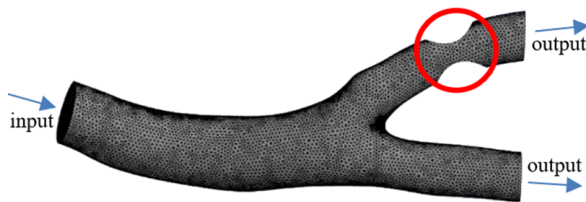

Figure 2: 3D mask of ischemic branch retinal artery occlusion.

Various mathematical models of blood flow in vascular constrictions have been developed in the last decades. These models revealed numerous hidden characteristics of blood flow, such as fluid behavior and flow properties [19]. Many studies focus on mathematical models to analyze the effect of stenosis on flow patterns, velocity, pressure, and shear stress, by delving into the degree of emergent disease stenosis. Roy et al. [26] document how blood flow patterns in the arterial stenosis of the heart. Andayesh [3] also explores the flow patterns in stenosed renal arteries based on the degree of stenosis and branching angle. Another study by Ali et al. [2] discuss a mathematical model to examine blood flow through a blocked cylindrical blood vessel of the heart. A model for blood flow in cardiovascular disease in cardiac arteries in terms of the simultaneous influence of the geometric shape of the stenosis has been developed by Kumar et al. [15].

Despite the existing lines of inquiry, more research is called upon to further examine the blood flow through stenosed or blocked arteries, in light of advancing biomedical applications. The cumulative effect of physical properties can be helpful in understanding such observations. To our knowledge, there has been no research on blood flow in the vasoconstriction in the retinal arteries of the eye, especially in cases of BRAO. Therefore, this research seeks to develop a mathematical model devoted to examining BRAO. This objective is closely related to the degree of constriction and the initial velocity of blood flow, and it is projected to shed light on the following underresearched area:

1. Simultaneous effect of blood flow at various degrees of stenosis in BRAO cases.

2. Simultaneous effect of blood flow on various degrees of initial flow velocity in BRAO cases.

3. Clustering the ANSYS simulation results using K-Means Clustering into a bar chart form makes it easier for researchers to classify velocity, pressure, and wall shear stress.

1.1   Mathematical model

Several internal and external factors cause stenosis of the retinal blood vessels. This numerical simulation helps the medical research community determine the internal factors driving wall stenosis and often enable the determination of flow variable which is difficult to obtain through experiments, e.g. wall shear stresses [25]. To support the analysis of the stenosis and identify the ischemic site, the geometry of the stenosis is put under investigation, and a diagram is created, as shown in Figure 3. The working fluid refers to blood, which has the properties of a Newtonian fluid, incompressible, unsteady, and turbulent.
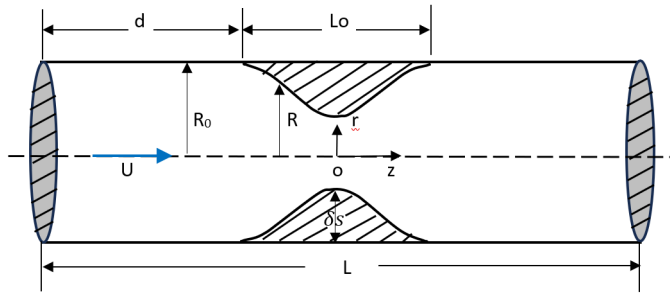
Figure 3: Flow geometry of the stenosed tube.

The equations governing the boundary conditions for simulating the hydrodynamics of blood flow in BRAO are defined as follows,

$$\frac{\partial u_i}{\partial x_i} = 0,\tag{1}$$

$$\frac{\partial \rho u_i}{\partial t} + \frac{\partial \rho u_i u_j}{\partial x_j} = -\frac{\partial P}{\partial x_i} + \mu \frac{\partial^2 u_i}{\partial x_i{}^2}.\tag{2}$$

Pralhad and Schultz [9, 24] express the mathematical formula for the geometry of the stenosis that is assumed to be symmetrical is given by,

$$R(z) = \begin{cases} R_0 - \dfrac{\delta s}{2}\left(1 + \cos\dfrac{2\pi}{Lo}\left(z - d - \dfrac{Lo}{2}\right)\right), & d \le z \le d + Lo, \\ R_0, & \text{others}, \end{cases}\tag{3}$$

where

$$\begin{aligned}
R(z) &= \text{radius on stenosis,} \\
R_0 &= \text{the arterial radius,} \\
\delta s &= \text{the maximum height of the stenosis,} \\
L &= \text{the arterial length,} \\
Lo &= \text{the total length of the stenosis,} \\
z &= \text{flow direction,} \\
d &= \text{stenosis location,} \\
u &= v = 0; \quad \text{at the arterial wall } (r = R(z)).
\end{aligned}$$

The literature [26] shows that the stenosed artery wall is considered rigid and immobile. When flowing, the friction between the fluid and the wall is negligible at the wall, so the pressure gradient normal to the wall is assumed to be zero. Roy et al. [26] explains the velocity of fluid flowing in a narrowed channel as follows,

$$u = 2U_0\left(1 - \left(\frac{r}{R(z)}\right)^2\right), \quad \text{at the inlet (at } z = 0).\tag{4}$$

Pousielle's law [7, 10] states that fluid flow through a cylindrical pipe with length L and trans-

verse radius r can be determined by the formula,

$$Q = \frac{\pi \Delta P r^4}{8 \eta L}. \tag{5}$$

With ΔP is the pressure gradient, η is the viscosity of the fluid, L is the length of tube, Q is the flow, r is the radius of tube.

2 Methodology

The Navier-Stokes equations (1) and continuity (2) were used to calculate the velocity and pressure field in the stenotic of the retinal artery branch. The finite volume method (FVM) was used to discretize the above-mentioned equations [29]. To solve the fluid flow equation, we used the Quadratic Upstream Interpolation for Convective Kinetics (QUICK) algorithm as Figure 4. This algorithm uses three-point upstream weighted square interpolation for cell face values. The face value $\emptyset$ was obtained from a quadratic function passing through two bracketing nodes (on each side of the face) and a node on the upstream side [20].
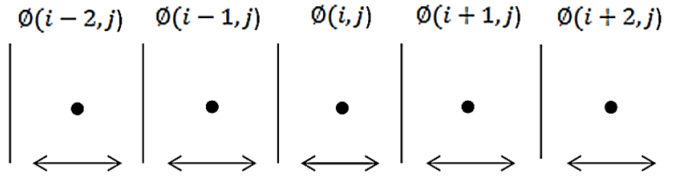

Figure 4: Discretization of QUICK method.

$$\emptyset_e(i,j) = \emptyset(i,j) + g_1(\emptyset(i+1,j) - \emptyset(i,j)) + g_2(\emptyset(i,j) - \emptyset(i-1,j)). \tag{6}$$

Note that:

$$g_1 = \frac{\left[\emptyset_e(i,j) - \emptyset(i,j)\right]\left[\emptyset_e(i,j) - \emptyset(i-1,j)\right]}{\left[\emptyset(i+1,j) - \emptyset(i,j)\right]\left[\emptyset(i+1,j) - \emptyset(i-1,j)\right]}, \tag{7}$$

$$g_2 = \frac{\left[\emptyset_e(i,j) - \emptyset(i,j)\right]\left[\emptyset(i+1,j) - \emptyset_e(i,j)\right]}{\left[\emptyset(i+1,j) - \emptyset(i,j)\right]\left[\emptyset(i+1,j) - \emptyset(i-1,j)\right]}. \tag{8}$$

Substitute (7) and (8) into (6), which is displayed as follows:

$$\emptyset_e(i,j) = -\frac{1}{8}\emptyset(i-1,j) + \frac{3}{4}\emptyset(i,j) + \frac{3}{8}\emptyset(i+1,j), \tag{9}$$

$$\emptyset_w(i,j) = -\frac{1}{8}\emptyset(i-2j) + \frac{3}{4}\emptyset(i-1,j) + \frac{3}{8}\emptyset(i,j). \tag{10}$$

The next step was to discretize the branch retinal artery blood vessels into linear equations that would be solved using MATLAB. ANSYS Fluent (version 2024R1, ANSYS Inc.) was used to solve the turbulence model of Newtonian fluid flow at BRAO, which involved dividing the simulation domain into a series of small interconnected volumes or control cells. Variable values (velocity and pressure) were then calculated at the center of mass of these cells. ANSYS Fluent employed an iterative algorithm to solve these equations until a convergent solution was obtained The simulation time step size was set to 0.1 seconds by running 200-step iterations. The next step was to analyze the simulation results with the aid of the ANSYS application to draw further conclusions.

Image segmentation aided in classifying images into different groups. One technique in image segmentation is clustering. In this research, the K-means grouping algorithm was used to interpret images from Computational Fluids Dynamics (CFD) simulation results and group them into k groups of images [8, 28]. For example, there was an image with $x \times y$ resolution, and the image was grouped into k number of clusters. Let $p(x, y)$ be the input pixel to be used as a cluster and c_k be the cluster center. The algorithm for k-means clustering [21] was defined as follows:

1. Initialize the number of clusters k and centers.

2. For each pixel in the image, calculate the Euclidean distance d between the image center and each pixel by using the following formula,

$$||d = p(x, y) - c_k||. \tag{11}$$

3. Assign all pixels to the nearest center based on distance d.

4. After all pixels have been assigned, recalculate the new center position using the following formula,

$$c_k = \frac{1}{k} \sum p(x, y). \tag{12}$$

5. Repeat the process until the tolerance or error value is reached.

6. Convert the cluster pixels to an image.

7. Classify the resulting cluster images into a bar chart.

3   Results And Discussion

Table 1 presents the factors that influence blood flow rate in BRAO due to eye stroke [11, 6]. Numerical experiments were carried out for flow through a stenotic artery with variations in blockage and volume reduction of 45%, 60%, 75%, and 90%.

Table 1: Parameters values regarding factors that influence blood flow rate in BRAO.

Parameter	Value
Diameter renal artery	$265 \pm 20\mu m$
Blood density	$1.054 - 1.060kg/m^3$
Viscosity	$0.003kg/ms$
Hypertensive blood pressure	$Systolic :> 140mmHg$
	$Diastolic :> 90mmHg$
Velocity artery	$0.19 - 0.49m/s$
Initial Velocity	$0.3m/s$
Pressure	$17331Pa$
Thermal Conductivity	$0.44W/mK$

The numerical simulation results demonstrated how thickness influenced the blood flow rate in BRAO. In the first simulation, a thickness percentage of 45% of the Retinal Artery branch diameter ($119\mu m$) was used. The second simulation used 60% of the Retinal Artery branch diameter

(159μm). The third one used 75% (199μm). The last simulation used 90% (238μm). The simulation results (refer to Figure 5) indicate that the flow velocity in the area prior to the stenosis has a standard blood velocity and continues to rise towards the central area of the stenosis. Outside the central region of constriction, the flow velocity begins to decrease as the flow cross-sectional area gradually increases. Numerical simulation results demonstrate that the greater the thickness of the clot, the greater the blood flow rate. With a thickness of 90%, the blood flow rate has exceeded the standard flow rate limit (> 0.49 m/s), which makes the blood vessels prone to rupture.

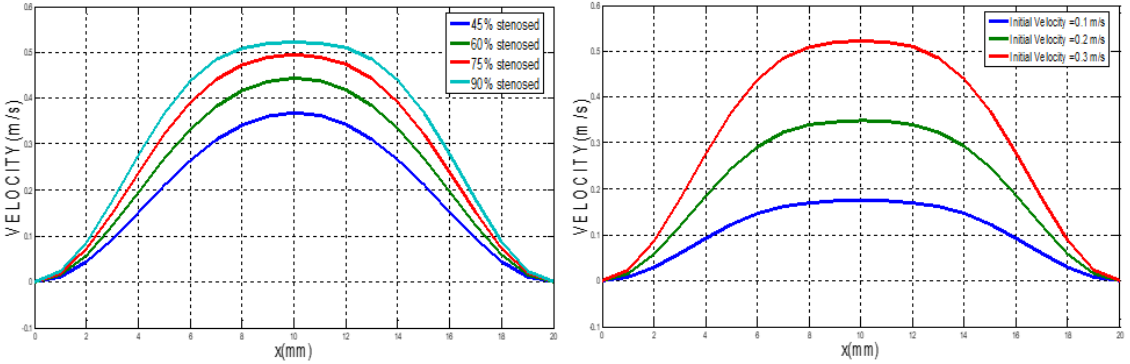Figure 5: The numerical simulation results of flow velocity in BRAO: (**a**) Based on thickness of stenosis. (**b**) Based on initial flow velocity.

The second numerical simulation aimed to determine the effect of thickness on fluid flow pressure. This simulation applied the same thickness level as the previous simulation. Figure 6 depicts that the variation of pressure for various inputs with $R_0 = 1$, $L = 10\mu m$, and $L_0 = 100\mu m$. Based on the simulation results, it can be seen that the area before the stenosis has high pressure (17522 Pa) and continues to fall toward the central area of the stenosis (17270 Pa). Outside the central region of stenosis, the pressure begins to increase as the flow cross-sectional area gradually increases. For stenosis thickness $\delta s = 238\mu m$ (90%), the blood flow pressure fluctuations are quite large, ranging from $17270 - 17522$ Pa, while the smallest fluctuations occur for clot thickness $\delta s = 119\mu m$ (45%), which is $17327 - 17466$ Pa (refer to Table 2). This coheres with research conducted by Roy et al. [26] and Ali et al. [2], noting that the pressure in the blood vessels before the stenosis area tends to be high, which subsequently decreases towards the center of the stenosis. This pressure is presumed to increase again in areas away from the center of stenosis. The greatest intensity of stenosis occurs in the area with the highest degree of narrowing.
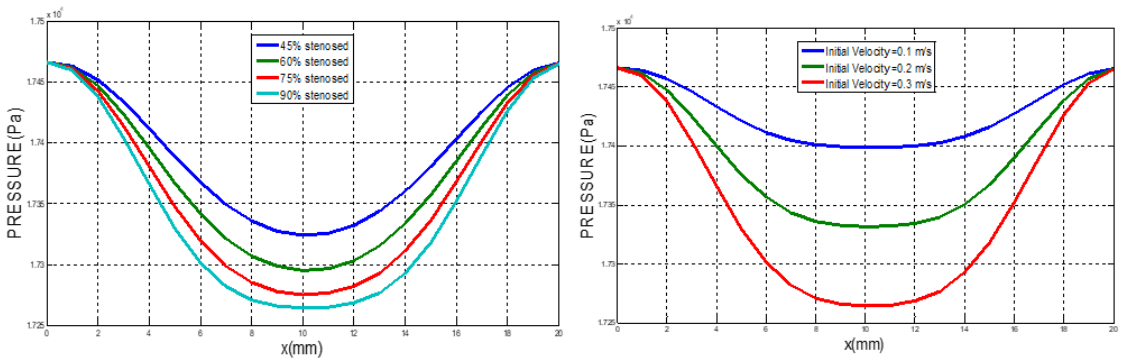

Figure 6: The numerical simulation results of pressure in BRAO: (**a**) Based on thickness of stenosis. (**b**) Based on initial flow velocity.

Table 2: Numerical simulation results for flow velocity, pressure and wall share based on thickness level.

Thickness level	Velocity	Pressure	Wall Shear
$45\%(119\mu m)$	$0.006 - 0.439 m/s$	$17327 - 17466 Pa$	$1.425 - 9.928 Pa$
$60\%(159\mu m)$	$0.010 - 0.439 m/s$	$17327 - 17494 Pa$	$1.425 - 11.345 Pa$
$75\%(199\mu m)$	$0.015 - 0.494 m/s$	$17299 - 17494 Pa$	$1.425 - 11.345 Pa$
$90\%(238\mu m)$	$0.055 - 0.549 m/s$	$17270 - 17522 Pa$	$1.425 - 14.179 Pa$

Figures 7 and 8 show the velocity distribution at the inlet and outlet channels in BRAO with different levels of stenosed area. The velocity continues to increase until it reaches the location of maximum stenosis. In simulations 7(b) and 7(c), with a stenosis level of $45\% - 60\%$, respectively, the turbulent flow has not occurred in the stenosis area, and the flow velocity remains normal. In the second simulation, 7(d), with a stenosis level of 75%, turbulent flow appears in the stenosis area, but the velocity remains normal. For a 90% stenosis, the velocity has exceeded the standard limit of blood flow velocity. Extremely high velocity, associated with over 90% stenosis, is believed to cause fatal outcomes.
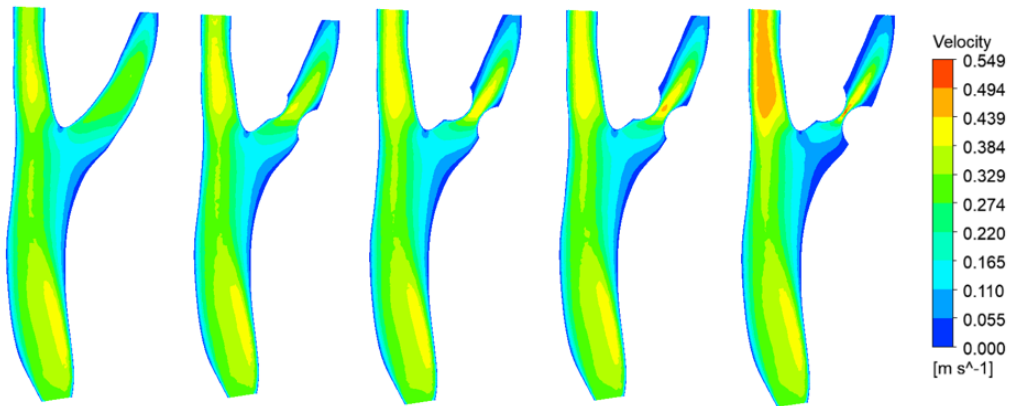

Figure 7: Flow vector plots in planes in the fluid domain for a non-deformed and stenotic retinal vessel model when a flow rate of 0.3m/s at the inlet is applied: (**a**) Non stenosis. (**b**) 45% stenosed. (**c**) 60% stenosed. (**d**) 75% stenosed. (**e**) 90% stenosed.
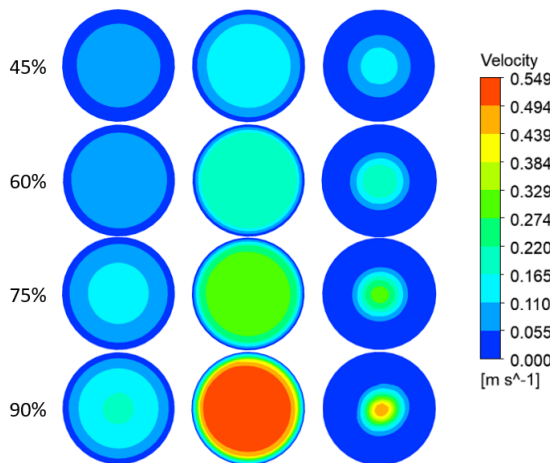

Figure 8: Velocity in pre-stenosis, stenosis center, and post-stenosis with stenosis ranging from 45% to 90%.

The pressure contour on the surface of the retinal artery branch is shown in Figure 9. For all cases, the maximum pressure occurs at the inlet of the blood vessel, which then hits the branch wall and separates into two streams. A low-pressure area characterizes the stenosis area, while the upstream area has higher pressure. As shown in Figure 7, the flow velocity continues to increase until it reaches the location of maximum stenosis. By implication, as blood flows at an increasingly higher velocity, this causes an increasing negative pressure gradient in that direction. Therefore, the area before the stenosis will have a higher pressure, yet the pressure will continue to decline until it reaches the central area of stenosis. The pressure will increase as the resistance in the blood flow area increases. In regions beyond the central stenosis, there is a gradual increase in pressure as the flow cross-sectional area begins to expand. The pressure contours in the BRAO cases are shown in Figure 9. For all cases, the maximum pressure occurs at the bifurcation region as the blood flow hits it and separates into two streams. A low-pressure region characterizes the stenosis region, while the upstream part has a higher pressure. The flow velocity continues to increase until maximum stenosis, as shown in Figure 9. As a result, when blood flows at a higher velocity, the negative pressure gradient rises in that direction. Therefore, the pressure will increase upstream of the stenosis and drop until the maximum stenosis is reached-the maximum pressure increases along with the obstruction in the flow area. The pressure rises again when the flow increases gradually beyond the maximum stenosis.
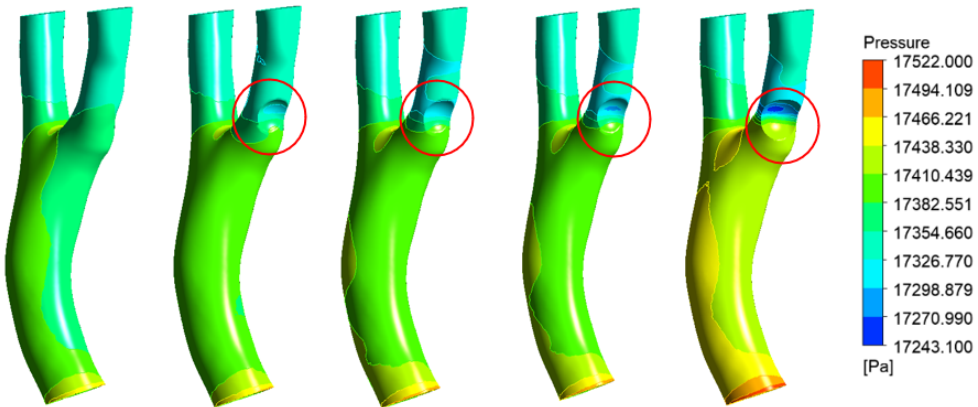

Figure 9: The pressure on the surface of a model of non-deformed and stenosed retinal vessels: (**a**) Non stenosis. (**b**) 45% stenosed. (**c**) 60% stenosed. (**d**) 75% stenosed. (**e**) 90% stenosed.
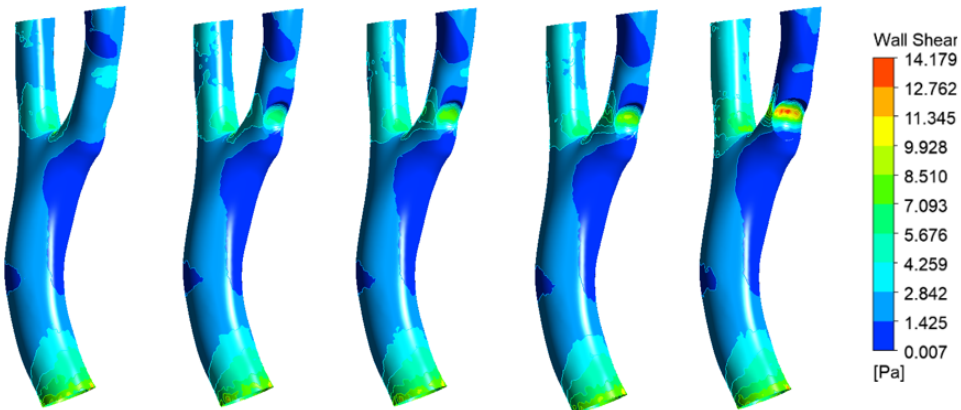

Figure 10: Plot of wall shear on the surface of a model of non-deformed and stenosed retinal vessels: (**a**) Non stenosis. (**b**) 45% stenosed. (**c**) 60% stenosed. (**d**) 75% stenosed. (**e**) 90% stenosed.

The contours of the wall shear stress at the stenosed retinal artery bifurcation are shown in Figure 10. Based on the simulation results, as the degree of stenosis increases, the wall shear stress also increases in the stenosis area. At $45\% - 75\%$ stenosis, the magnitude of wall shear stress ranges from 5.6 to 9.9 Pa; at 90% stenosis, there is a considerable increase in wall shear stress, ranging from 9.9 to 14.1 Pa. This results from the increase in overall geometric curvature as the effect of the stenosis further reduces the volume of the domain by pushing against it.
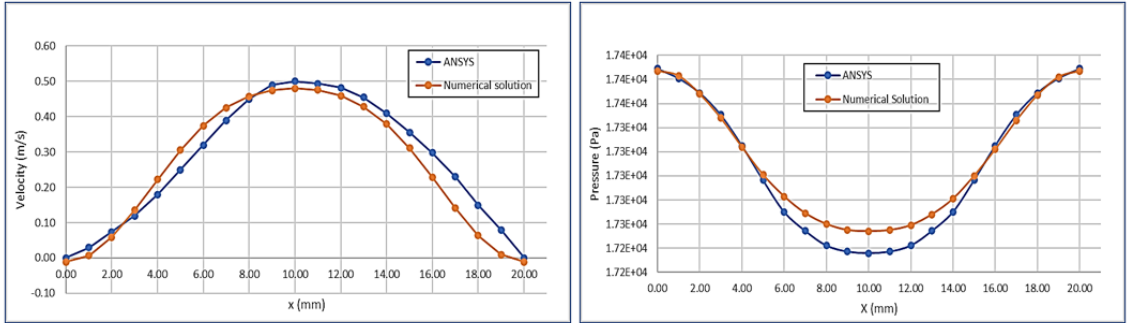

Figure 11: Comparison of ANSYS results and numerical results of blood flow velocity and pressure in BRAO.

In general, the comparison of simulation results between the numerical solution using the SIMPLE algorithm and ANSYS demonstrates the same trend. Figures 11 indicate a satisfactory coherence between the numerical and ANSYS calculations.

3.1   Cluster size distribution

The image segmentation with K-Means clustering for two domains (refer to Figures 7 and 9), starting from a stenosis level of 0% to 90%, is shown in Figures 4 and 5. When the blob thickness level increases, the cluster's contribution to the more significant one increases due to the emergence of turbulent flow. This occurs in both domains (refer to Figures 6 and 7), namely flow velocity and pressure in BRAO. The distribution of cluster size for each domain is shown in Figures 8 and 9.

Figure 12 shows the clusterization results of flow velocity based on CFD simulation results with different levels of constriction. This clusterization is processed from the CFD simulation results in Figure 12 by using the K-Means clustering method. Figure 7 illustrates that at 45% stenosis, there is a peak in the population at 0.329 m/s, but the emergent cluster remains unchanged. However, for a population at a rate of $0.494 - 0.549$ m/s, this does not occur. The clusterization results for a stenosis level of 60% are fairly similar to those in the previous stenosis level, in that not all clusters appear in population numbers, and cluster types at the speed of $0.494 - 0.549$ m/s do not appear. The clusterization results for a stenosis level of 75% give rise to a new cluster type, 0.494 m/s. The number of cluster populations has begun to decline for the low-flow category cluster type, along with the emergence of new clusters. In the last level of clusterization with a stenosis of 90%, the population of high-paced flows is 0.549 m/s. These results imply that stenosis of 90% gives rise to various types of clusters, ranging from low to high levels. As a corollary, this leads to velocity fluctuations that approach variable stenosis (turbulent flow).
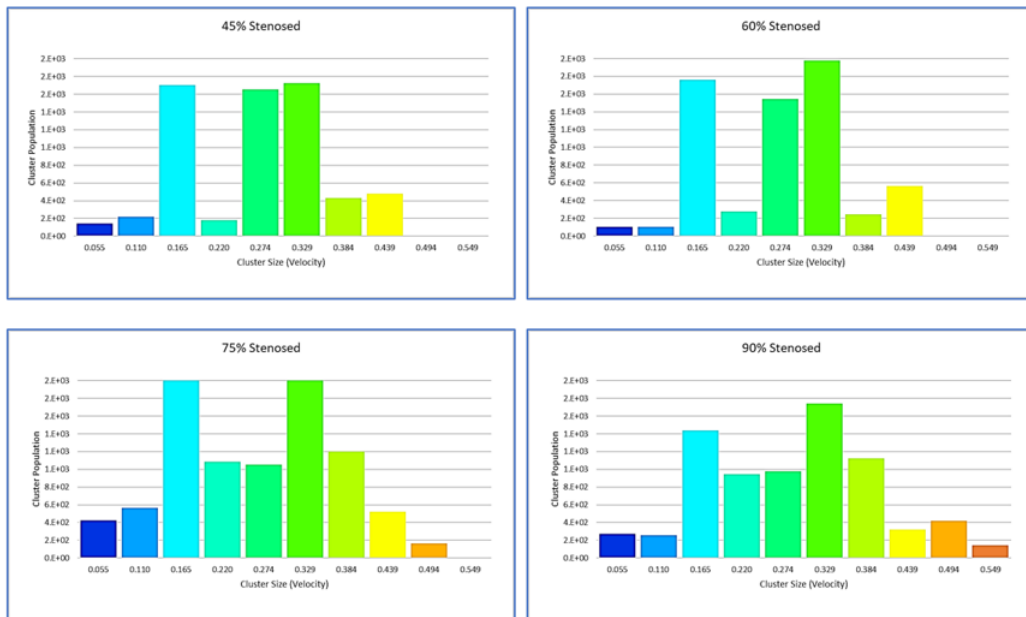
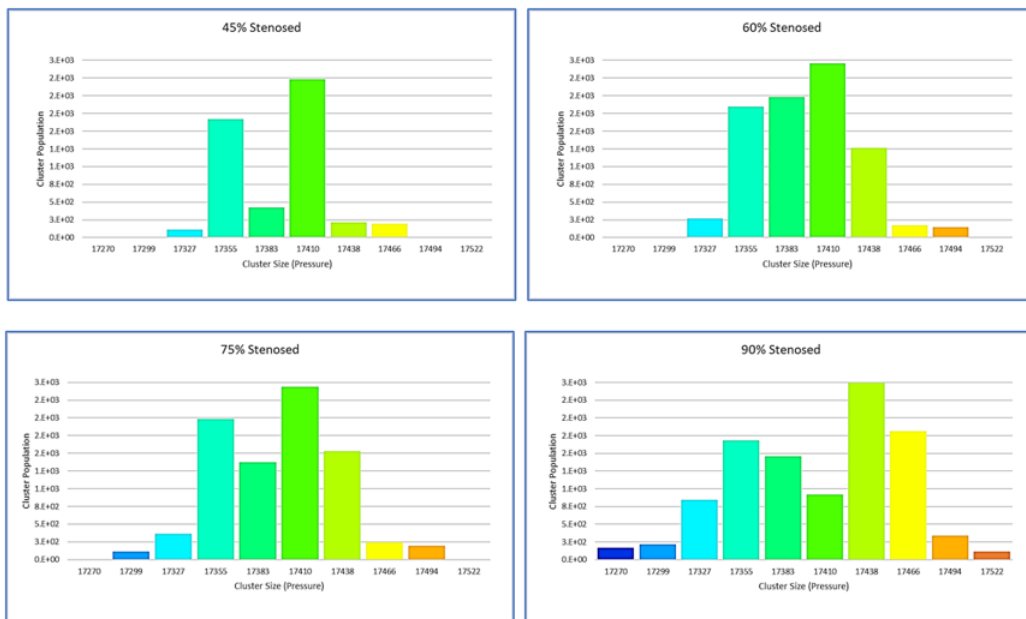Figure 12: Comparison of velocity with different levels of stenosis.

Figure 13: Comparison of pressure with different levels of stenosis.

Figure 13 shows the clusterization results of flow pressure based on CFD simulation results with different levels of constriction. This clusterization is processed from the CFD simulation results in Figure 9 using the K-Means clustering method. Figure 13 shows that the initial form (non-stenosis) has a uniform cluster, namely between 17342 and 17451 Pa, with a peak population at a pressure size of 17397 Pa. The clusterization results for a 20% stenosis level show minimal

differences from the previous level, with not all types of clusters appearing in the population numbers, and a cluster at the pressure size of $17315 - 17478$ Pa emerging at the population peak of 17397 Pa. The clusterization results in a stenosis level of 35%, giving rise to a new interval, namely $17315 - 17506$ Pa, with a peak population of 17424 Pa. In the results of the last level of clusterization with a stenosis of 50%, a population of varying flow pressures emerges, where each cluster size appears between 17287 and 17553 Pa with a peak population of 17451 Pa. This indicates that a 50% stenosis leads to various types of clusters ranging from low to high levels (turbulent flow), resulting in varying pressure fluctuations on the walls experiencing stenosis.
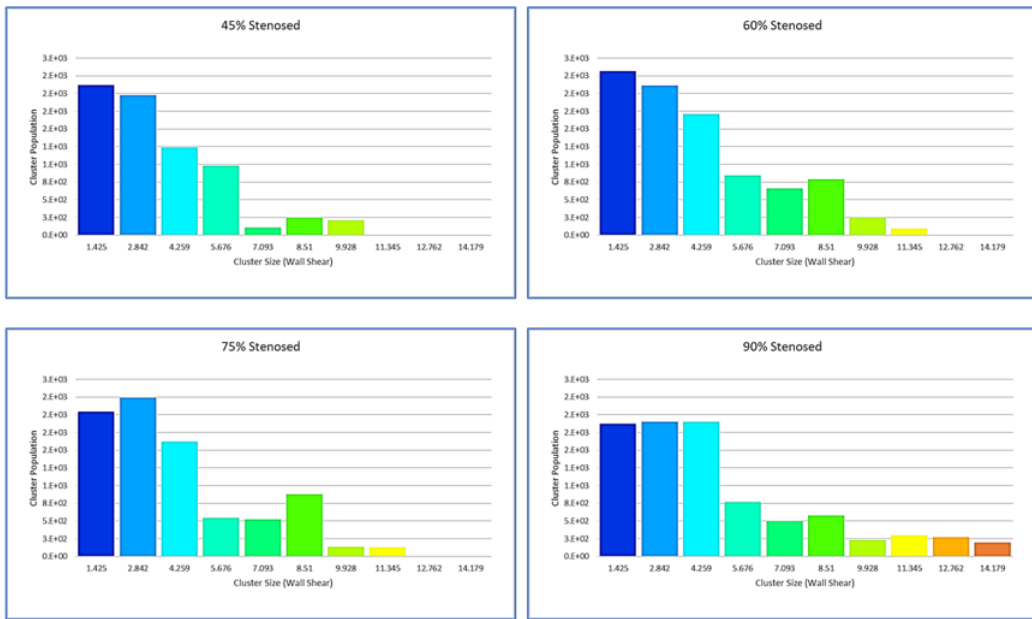

Figure 14: Comparison of wall shear with different levels of stenosis.

Figure 14 shows the clustering results of the wall shear stress in the BRAO case. At the 45% constriction level, the wall shear stress ranges from 1425 to 9928 Pa. This value increases as the constriction increases from 60% to 75%, ranging from 1425 to 11345 Pa. The last level of clustering results in 90% stenosis, leading to various types of clusters from low to high levels, ranging from 1425 to 14179 Pa. When the shear stress in blood vessels is high, it has several negative impacts on blood vessel health, including causing damage to the endothelial layer of blood vessels, which can trigger an inflammatory response and atherosclerosis (vasoconstriction due to plaque buildup). In addition, high shear stress can increase the risk of blood clot formation (thrombosis). It can cause structural damage to the blood vessel wall, such as rupture of the blood vessel wall or the formation of aneurysms (swelling of the blood vessel wall that is at risk of rupture).

Our study has several limitations that need to be addressed. Firstly, our mathematical model assumes a rigid wall for a realistic retinal artery branch, which includes pre-stenosis, stenosis center, and post-stenosis segments. We believe that it would be more accurate to use an elastic wall model with explicit dynamics to better reflect physiological conditions. Secondly, with respect to realistic constriction position, future research is advised to engage a BRAO model with more realistic geometry, to evaluate the effects of constriction position. Third, in this study, the geometry of the constriction uses a bell-shaped and symmetrical model. Further research needs to involve other geometric shapes such as elliptical and trapezoidal. A final recommendation is to examine

the circumstances where the constriction geometry is asymmetrical and the shapes of the upper and lower constrictions are different.

4   Conclusions

This study has simulated the effect of constriction on BRAO in ocular stroke cases and examined how it affects flow characteristics. It has also validated a mathematical blood flow model through stenotic retinal arteries over a wide range of stenosis levels, from 45% to 90%. Detailed findings from the study are hereby presented:

- Numerical simulations and CFD results show that 90% stenosis in arteries can be highly harmful, leading to a transition in flow pattern from turbulent to laminar flow.

- With the increased severity of stenosis, the pressure and wall shear stress at the stenosis region also increase, eventually and the high-speed flow rate formed at the stenosed region begins to dominate the flow.

- The velocity and pressure drop increase progressively as the degree of stenosis intensifies, highlighting the importance of early intervention.

- The wall shear stress is significantly higher in the stenosis section.

This analysis is believed to provide valuable insights into CVD and assist health researchers in their knowledge of blood flow profiles in BRAO cases. It has also contributed to a more fine-cut understanding of the impact of BRAO on eye stroke. In addition, by determining the thickness and length of stenosis narrowing in the retinal artery blood flow, researchers can predict when the retinal blood vessels will rupture, which can cause eye stroke. For future research, the authors propose the following areas of potential inquiry:

- Mathematically modeling the effect of the branching angle for the BRAO case.

- Correlation between branching angle and non-Newtonian fluid flow pattern for BRAO case.

- Asymmetrical geometry of the stenosis.

- The analysis of stenosis using hemodynamic parameters, such as the time-dependent wall shear stress.

- Future research could apply and compare the findings of this study with experimental results.

Conflicts of Interest The authors declare that we have no conflicts of interest to reveal.

References

[1] S. N. A. M. Abidin, N. A. Jaafar & Z. Ismail (2023). Exact analysis of unsteady solute dispersion in blood flow: A theoretical study. *Malaysian Journal of Mathematical Sciences*, 17(3), 349–361. https://doi.org/10.47836/mjms.17.3.07.

[2] A. Ali, M. Hussain, M. S. Anwar & M. Inc (2021). Mathematical modeling and parametric investigation of blood flow through a stenosis artery. *Applied Mathematics and Mechanics*, 42(11), 1675–1684. https://doi.org/10.1007/s10483-021-2791-8.

[3] M. Andayesh, A. Shahidian & M. Ghassemi (2020). Numerical investigation of renal artery hemodynamics based on the physiological response to renal artery stenosis. *Journal of Applied Biomedicine*, 40(4), 1458–1468. https://doi.org/10.1016/j.bbe.2020.08.006.

[4] J. R. Cebral, F. Mut, M. Raschi, E. Scrivano, R. Ceratto, P. Lylyk & C. M. Putman (2011). Aneurysm rupture following treatment with flow-diverting stents: computational hemodynamics analysis of treatment. *American Journal of Neuroradiology*, 32(1), 27–33. https://doi.org/10.3174/ajnr.A2398.

[5] A. V. Chobanian, G. L. Bakris, H. R. Black, W. C. Cushman, L. A. Green, J. L. Izzo Jr, D. W. Jones, B. J. Materson, S. Oparil, J. T. Wright Jr, E. J. Roccella & N. H. B. P. E. P. C. Committee (2004). The seventh report of the joint national committee on prevention, detection, evaluation, and treatment of high blood pressure: The JNC 7 report. *JAMA*, 289(19), 2560–2571. https://doi:10.1001/jama.289.19.2560.

[6] G. De Salvo, M. Oshallah, A. E. Sepetis, R. Borbara, G. W. Oliverio, A. Meduri, R. Frisina & A. Jacob (2023). Inner retinal thinning comparison between branch retinal artery occlusion and primary open-angle glaucoma. *Diagnostics*, 13(22), Article ID: 3428. https://doi.org/10.3390/diagnostics13223428.

[7] W. Deng & K. I. Tsubota (2022). Numerical simulation of the vascular structure dependence of blood flow in the kidney. *Medical Engineering & Physics*, 104(1), Article ID: 103809. https://doi.org/10.1016/j.medengphy.2022.103809.

[8] N. Dhanachandra, K. Manglem & Y. J. Chanu (2015). Image segmentation using k-means clustering algorithm and subtractive clustering algorithm. *Procedia Computer Science*, 54, 764–771. https://doi.org/10.1016/j.procs.2015.06.090.

[9] A. Fatahillah, S. Setiawani, A. S. Mandala, S. Suharto, R. P. Murtikusuma, L. N. Safrida, S. Hussen & R. Adawiyah (2019). Numerical analysis of blood flow in intracranial artery stenosis affected by ischemic stroke using finite element method. *Journal of Physics: Conference Series*, 1218(1), Article ID: 012005. https://doi:10.1088/1742-6596/1218/1/012005.

[10] F. Fiorillo, L. Esposito, M. Ginolfi & G. Leone (2024). New insights into turbulent and laminar flow relationships using Darcy–Weisbach and Poiseuille laws. *Water*, 16(10), Article ID: 1452. https://doi.org/10.3390/w16101452.

[11] D. Goldenberg, J. Shahar, A. Loewenstein & M. Goldstein (2013). Diameters of retinal blood vessels in a healthy cohort as measured by spectral domain optical coherence tomography. *Retina*, 33(9), 1888–1894. https://doi.org/10.1097/iae.0b013e31829477f2.

[12] S. S. Hayreh, P. A. Podhajsky & M. B. Zimmerman (2009). Branch retinal artery occlusion: Natural history of visual outcome. *Ophthalmology*, 116(6), 1188–1194.e4. https://doi.org/10.1016/j.ophtha.2009.01.015.

[13] S. S. Hayreh & M. B. Zimmerman (2007). Fundus changes in central retinal artery occlusion. *Retina*, 27(3), 276–289. https://doi.org/10.1097/01.iae.0000238095.97104.9b.

[14] J. J. Kanski (2020). *Clinical Ophthalmology: A Systematic Approach*. Elsevier Science Limited, London.

[15] S. Kumar & S. Kumar (2023). Blood flow with heat transfer through different geometries of stenotic arteries. *Trends in Sciences*, 20(11), Article ID: 6965. https://doi.org/10.48048/tis.2023.6965.

[16] F. Lauda, H. Neugebauer, L. Reiber & E. Jüttler (2015). Acute silent brain infraction in monocular visual loss of ischemic origin. *Cerebrovascular Diseases*, 40(3–4), 151–156. https://doi.org/10.1159/000437274.

[17] P. C. Lavallée, L. Cabrejo, J. Labreuche, M. Mazighi, E. Meseguer, C. Guidoux, H. Abboud, B. Lapergue, I. F. Klein, J. M. Olivot, G. Sirimarco, J. Gonzales-Valcarcel, P.-J. Touboul & P. Amarenco (2013). Spectrum of transient visual symptoms in a transient ischemic attack cohort. *Stroke*, 44(12), 3312–3317. https://doi.org/10.1161/strokeaha.113.002420.

[18] J. A. Leavitt, T. A. Larson, D. O. Hodge & R. E. Gullerud (2011). The incidence of central retinal artery occlusion in Olmsted County, Minnesota. *American Journal of Ophthalmology*, 152(5), 820–823.e2. https://doi.org/10.1016/j.ajo.2011.05.005.

[19] K. W. Lee & X. Y. Xu (2002). Modelling of flow and wall behaviour in a mildly stenosed tube. *Medical Engineering & Physics*, 24(9), 575–586. http://dx.doi.org/10.1016/S1350-4533(02)00048-6.

[20] D. Lopes, R. Agujetas, H. Puga, J. Teixeira, R. Lima, J. P. Alejo & C. Ferrera (2021). Analysis of finite element and finite volume methods for fluid-structure interaction simulation of blood flow in a real stenosed artery. *International Journal of Mechanical Sciences*, 207, Article ID: 106650. https://doi.org/10.1016/j.ijmecsci.2021.106650.

[21] A. S. Nasution, A. Alvin, A. T. Siregar & M. S. Sinaga (2022). KNN algorithm for identification of tomato disease based on image segmentation using enhanced k-means clustering. *KINETIK: Game Technology, Information System, Computer Network, Computing, Electronics, and Control*, 7(3), 299–308. https://doi.org/10.22219/kinetik.v7i3.1486.

[22] P. Nugroho, H. Andrew, K. Kohar, C. A. Noor & A. L. Sutranto (2022). Comparison between the world health organization (WHO) and international society of hypertension (ISH) guidelines for hypertension. *Annals of Medicine*, 54(1), 837–845. https://doi.org/10.1080/07853890.2022.2044510.

[23] A. Pinna, A. Zinellu, R. Serra, G. Boscia, L. Ronchi & S. Dore (2023). Combined branch retinal artery and central retinal vein occlusion: A systematic review. *Vision*, 7(3), Article ID: 51. https://doi.org/10.3390/vision7030051.

[24] R. N. Pralhad & D. H. Schultz (2004). Mmodeling of arterial stenosis and its applications to blood diseases. *Mathematical Biosciences*, 190(2), 203–220. https://doi.org/10.1016/j.mbs.2004.01.009.

[25] C. Rajashekhar, G. Manjunatha & B. Fabian (2017). Finite element simulation of blood flow through an artery bifurcation: A mathematical model. *Malaysian Journal of Mathematical Sciences*, 11(2), 165–179.

[26] M. Roy, B. S. Sikarwar, M. Bhandwal & P. Ranjan (2017). Modelling of blood flow in stenosed arteries. *Procedia Computer Science*, 115, 821–830. https://doi.org/10.1016/j.procs.2017.09.164.

[27] D. Scoles, B. McGeehan & B. L. VanderBeek (2022). The association of stroke with central and branch retinal arterial occlusion. *Eye*, *36*(4), 835–843. https://doi.org/10.1038/s41433-021-01546-6.

[28] A. Varghese, S. Jain, M. Jawahar & A. A. Prince (2023). Auto-pore segmentation of digital microscopic leather images for species identification. *Engineering Applications of Artificial Intelligence*, *126*(C), Article ID: 107049. https://doi.org/10.1016/j.engappai.2023.107049.

[29] H. K. Versteeg & W. Malalasekera (2007). *An Introduction to Computational Fluid Dynamics: The Finite Volume Method*. Pearson Education, New York.